Nesting of the Fermi surface and the wave-vector-dependent susceptibility in quasi-one-dimensional electron systems

Yasumasa Hasegawa
Department of Material Science, Graduate School of Material Science, University of Hyogo, Hyogo 678-1297, Japan

Keita Kishigi
Faculty of Education, Kumamoto University, Kurokami 2-40-1, Kumamoto 860-8555, Japan

(Received 4 March 2010; revised manuscript received 24 May 2010; published 15 June 2010)

The wave-vector dependence of the susceptibility in quasi-one-dimensional systems is studied theoretically without and with external magnetic field in the perpendicular direction. We show that the wave-vector-dependent susceptibility has a two-step plateaulike structure in the absence of the magnetic field, when the warping of the Fermi surface caused by the $\mp 2\tau_3 \sin[3(k_y \mp \phi)]$ term, which breaks the reflection symmetry with respect to the most conducting chain, is larger than the critical value. The susceptibility is shown to have the plateaulike maximum in the small region in the wave vector at the edge of the lower plateau. We discuss the importance of the plateaulike maximum for the the field-induced spin density wave states in quasi-one-dimensional systems, such as the organic conductors $(TMTSF)_2PF_6$ and $(TMTSF)_2ClO_4$.

DOI: 10.1103/PhysRevB.81.235118 PACS number(s): 75.30.Fv, 78.30.Jw, 73.43.−f

I. INTRODUCTION

It is well known that while the static wave-vector-dependent susceptibility $\chi_0(\mathbf{Q})$ of the one-dimensional electron gas diverges logarithmically at $T=0$ when $|Q|=2k_F$, where k_F is the Fermi wave number, that of the two-dimensional electron gas has the constant value at $T=0$ when $|\mathbf{Q}| \leq 2k_F$. When the electrons are treated in the tight-binding approximation, the susceptibility depends on the shape of the Fermi surface. For the quasi-one-dimensional systems, where the Fermi surface is almost nested but the nesting is imperfect, the susceptibility has a plateaulike maximum in the region around the optimal nesting vector $\mathbf{Q}_0$.

The quasi-one-dimensional electron systems are realized in the organic superconductors $(TMTSF)_2X$, where $X=PF_6$ and ClO_4, in which a lot of interesting phenomena have been observed,[1,2] such as the conductivity depending on the direction of the magnetic field, superconductivity, quantum Hall effect in the bulk crystals, and field-induced spin density wave (FISDW).[3–10] The similar quasi-one-dimensional electron systems have been also realized in $(DMET\text{-}TSeF)_2X$ ($X=AuCl_2$, AuI_2).[11,12] The electron structure in the quasi-one-dimensional conductors such as $(TMTSF)_2X$ and $(DMET\text{-}TSeF)_2X$ is described by the 3/4 filled band of the tight-binding model in the triclinic lattice with the transfer integrals in the conducting plane as I_1, I_2, I_3, I_4, S_1 and S_2 (Fig. 1). We neglect the transfer integrals between planes. In $(TMTSF)_2ClO_4$, the noncentrosymmetric anions ClO_4 align alternatively in the b-direction and make the periodic potential, V, which we represent by the open and filled triangles in Fig. 1. Although this periodic potential plays an important role on the field-induced spin density waves,[13–21] we do not consider the effects of the anion ordering. In this paper we focus on the effect of the other nesting-breaking terms, i.e., the higher harmonic warpings of the Fermi surface breaking the reflection symmetry with respect to k_y, which have not been studied extensively. The transfer integrals and the warpings of the Fermi surface are expected to depend on the pressure. Therefore, the effects studied in this paper will be seen in experiments.

Since the transfer integrals along the chain (S_1 and S_2) are much larger than the hopping between the chains (I_1, I_2, I_3, and I_4), the Fermi surface consists with two warped planes near $k_x=\pm k_F=\pm 3\pi/4$.[1,2,22,23] Then we can linearize the energy with respect to k_x, and we obtain the model which is the extension of the model proposed by Yamaji.[1,24]

In this paper we study the nesting condition of the Fermi surface and the susceptibility in the absence of the magnetic field in detail. The relation between the susceptibility without magnetic field and that in the magnetic field is also discussed. We take the lattice constant to be 1 and $\hbar=c=1$.

II. QUASI-ONE-DIMENSIONAL FERMI SURFACE

A. Simple case on the square lattice

First we consider the simple case that the electrons are moving on the square lattice with only nearest neighbor hoppings t_a and t_b. This model has been used to study the properties of the quasi-one-dimensional electrons. In this simple model the energy is given by

$$\epsilon_{0\mathbf{k}} = -2t_a \cos k_x - 2t_b \cos k_y - \epsilon_F, \tag{1}$$

and the Fermi surface is given by $\epsilon_{0\mathbf{k}}=0$. In the quasi-one-dimensional system, t_a is much larger than t_b

$$t_a \gg t_b. \tag{2}$$

Then the Fermi surface is the two warped sheets given by

$$k_{0xF}(k_y) = \pm \arccos\left(\frac{-\epsilon_F}{2t_a} - \frac{t_b}{t_a}\cos k_y\right). \tag{3}$$

By series expansion in $t_b/t_a \ll 1$, we obtain the Fermi surface as

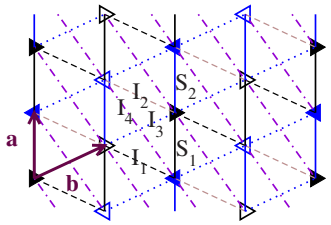

FIG. 1. (Color online) Triclinic lattice and transfer integrals in $(TMTSF)_2X$.

$$k_{0xF}(k_y) = \pm \left[k_F - \frac{1}{v_F} t_{0\perp}(k_y) \right], \tag{4}$$

where

$$t_{0\perp}(k_y) = -2t_1 \cos k_y - 2t_2 \cos 2k_y - 2t_3 \cos 3k_y - 2t_4 \cos 4k_y + \cdots . \tag{5}$$

In the above equation

$$\epsilon_F = -2t_a \cos k_F \left\{ 1 + O\left[\left(\frac{t_b}{t_a} \right)^2 \right] \right\}, \tag{6}$$

$$v_F = 2t_a \sin k_F \left\{ 1 + O\left[\left(\frac{t_b}{t_a} \right)^2 \right] \right\}, \tag{7}$$

$$t_1 = t_b \left\{ 1 + O\left[\left(\frac{t_b}{t_a} \right)^2 \right] \right\}, \tag{8}$$

$$t_2 = t_b' = O\left(\frac{t_b}{t_a} \right), \tag{9}$$

and

$$t_n = O\left[\left(\frac{t_b}{t_a} \right)^n \right]. \tag{10}$$

Then we obtain the linearized dispersion near the Fermi surface as

$$\tilde{\epsilon}_{0\mathbf{k}} = v_F(|k_x| - k_F) + t_\perp(k_y). \tag{11}$$

This model has been studied extensively in order to explain the FISDW states in the quasi-one-dimensional systems.[1–12,21,25–28]

B. Triclinic lattice

In the real systems the lattice is neither square nor rectangular in the plane (neither cubic nor tetragonal in the three-dimensional system) but triclinic. There are multiple transverse integrals I_1, I_2, I_3, I_4, S_1, and S_2 (see Fig. 1). In this case we linearize the dispersion with respect to k_x near the Fermi surface as

$$\epsilon_{\mathbf{k}}^{(R)} = v_F(k_x - k_F) + t_\perp^{(R)}(k_y), \tag{12}$$

$$\epsilon_{\mathbf{k}}^{(L)} = v_F(-k_x - k_F) + t_\perp^{(L)}(k_y), \tag{13}$$

where

$$t_\perp^{(R,L)}(k_y) = -2t_b \cos(k_y \mp \phi) - 2t_b' \cos[2(k_y \mp \phi)] \mp 2\tau_2 \sin[2(k_y \mp \phi)] - 2t_3 \cos[3(k_y \mp \phi)] \mp 2\tau_3 \sin[3(k_y \mp \phi)] - 2t_4 \cos[4(k_y \mp \phi)] \mp 2\tau_4 \sin[4(k_y \mp \phi)]. \tag{14}$$

The derivation is given in Appendix. In Eqs. (12)–(14), (R) and (L) mean $k_x \approx k_F$ and $k_x \approx -k_F$, i.e., the right and the left region in the momentum space, respectively, and $\mp$ means that $-$ or $+$ is taken for the right or the left region in the momentum space, respectively. In the above equation ϕ, t_b', t_3, t_4, τ_2, τ_3, and τ_4 come from several transfer integrals (S_1, S_2, S_3, S_4, I_1, and I_2) in the triclinic lattice. The term proportional to $\sin k_y$ does not exist, because this term can be included in ϕ, while τ_2, τ_3, and τ_4 terms are finite in general in the triclinic lattice. The imperfectness of the nesting of the Fermi surface are affected by the τ_2, τ_3, and τ_4 terms as well as t_b', t_3 and t_4 terms. In this paper we take

$$t_b'/t_b = 0.1, \tag{15}$$

and t_3, t_4, τ_2, τ_3, and τ_4 as parameters. Note

$$t_\perp^{(L)}(-k_y) = t_\perp^{(R)}(k_y), \tag{16}$$

$$\epsilon_{-\mathbf{k}} = \epsilon_{\mathbf{k}}, \tag{17}$$

due to time-reversal symmetry in the absence of a magnetic field.

III. NESTING VECTOR OF THE FERMI SURFACE

In the previous paper,[25] we studied the condition for the nesting vector $\mathbf{Q}$ in the quasi-one-dimensional systems in the rectangular lattice ($\tau_2=\tau_3=\tau_4=0$, $\phi=0$). Here we study the general case. The right and the left parts of the Fermi surface are given by

$$\epsilon_{\mathbf{k}}^{(R)} = 0, \tag{18}$$

and

$$\epsilon_{\mathbf{k}}^{(L)} = 0. \tag{19}$$

The Fermi surface is given by two warped curves $k_{xF}^{(R,L)}(k_y)$ as a function of k_y in the k_x-k_y plane, where

$$k_{xF}^{R,L}(k_y) = \pm \left(k_F - \frac{1}{v_F} t_\perp^{(R,L)}(k_y) \right). \tag{20}$$

When we translate the left part of the Fermi line with the nesting vector $\mathbf{Q}$, the translated line is given by

$$k_{xF}^{(L)\prime}(k_y) = Q_x - k_F + \frac{1}{v_F} t_\perp^{(L)}(k_y - Q_y). \tag{21}$$

When $t_b'=\tau_3=t_4=0$, the Fermi surface is perfectly nested with the vector $\mathbf{Q}_0$, where

$$\mathbf{Q}_0 = (2k_F, \pi + 2\phi). \tag{22}$$

We define $\mathbf{q}$ by

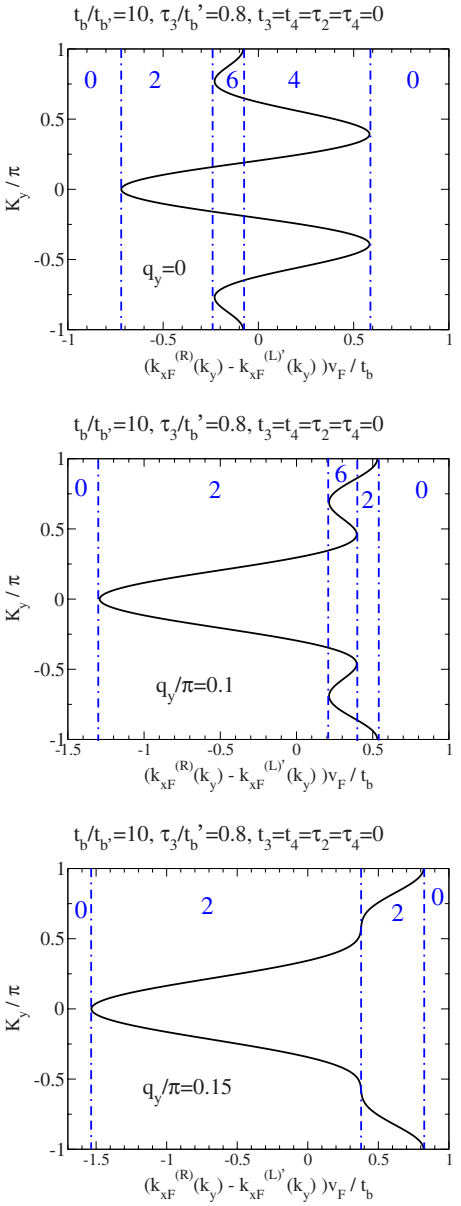

FIG. 2. (Color online) $k_{xF}^{(R)}(k_y)-k_{xF}^{(L)\prime}(k_y)$ vs K_y for $q_y/\pi=0$, 0.1 and 0.15.

$$\mathbf{q}=\mathbf{Q}-\mathbf{Q}_0, \tag{23}$$

and we obtain

$$k_{xF}^{(R)}(k_y)-k_{xF}^{(L)\prime}(k_y)=-q_x-[a_1\cos K_y+a_2\cos(2K_y)+a_3\cos(3K_y)+a_4\cos(4K_y)], \tag{24}$$

where

$$K_y=k_y-\frac{Q_y}{2}=k_y-\frac{1}{2}(q_y+\pi+2\phi), \tag{25}$$

$$a_1=\frac{4}{v_F}t_b\sin\frac{q_y}{2}, \tag{26}$$

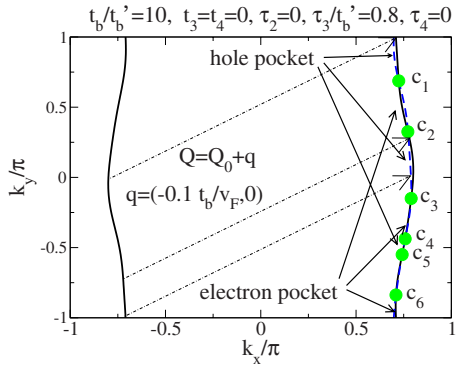

FIG. 3. (Color online) The intersection of the Fermi surface for parameters realizing six crossing points.

$$a_2=\frac{4}{v_F}(t_b'\cos q_y+\tau_2\sin q_y), \tag{27}$$

$$a_3=-\frac{4}{v_F}\left(t_3\sin\frac{3q_y}{2}-\tau_3\cos\frac{3q_y}{2}\right), \tag{28}$$

$$a_4=-\frac{4}{v_F}(t_4\cos 2q_y+\tau_4\sin 2q_y). \tag{29}$$

We examine the condition for intersection of the Fermi surface with the translation of **Q**. The condition for the intersection of the Fermi surface is given by

$$k_{xF}^{(R)}(k_y)-k_{xF}^{(L)\prime}(k_y)=0. \tag{30}$$

We take $q_x=0$ and the fixed value of q_y, and plot $k_{xF}^{(R)}(k_y)-k_{xF}^{(L)\prime}(k_y)$ vs K_y as shown in Fig. 2. If q_x (in the unit of t_b/v_F) is in the region labeled by "0," there are no intersection of the Fermi surface with the vector **Q**. If q_x is in the region labeled by "2," "4," or "6," the intersection of the Fermi surface with the translated one occurs "2," "4," or "6" times, respectively. Figure 3 shows the example for six crossing points. In this way we can plot the boundary for the different number of crossing points in the q_x-q_y plane (Fig. 4). We have shown[25] that when $\tau_2=\tau_3=\tau_4=0$, the region of the four crossing points is important in the quasi-one-dimensional system (we have called the region of the four crossing points as *swept back* region in the previous paper). We find that the new region of the six crossing points (region "6") appears if τ_3 is larger than the critical value $|\tau_3|\geq\tau_3^*$, while this region is not generated by the τ_2 term. The t_3 term also makes the region "6" but the area of that region is small, as we will show below. The critical value τ_3^* depends on other parameters, t_3, τ_2, etc. We obtain that $\tau_3^*\approx 0.19|t_b'|$, when $t_3=t_4=0$, $\tau_2=\tau_4=0$, and $t_b'=0.1t_b$. As shown in the Appendix, the estimated value of the parameter $|\tau_3/t_b'|$ for the organic conductor $(TMTSF)_2ClO_4$ is near the critical value. We plot the τ_3 dependence of the edge point of the region "6" in Fig. 5. As seen in Fig. 5, $|K_y|$ becomes π at $\tau_3=\tau_3^*$. When τ_3 is close to the critical value, the region "6" has very small area in q_x-q_y plane, but its area becomes larger as τ_3 becomes larger (see Fig. 4).

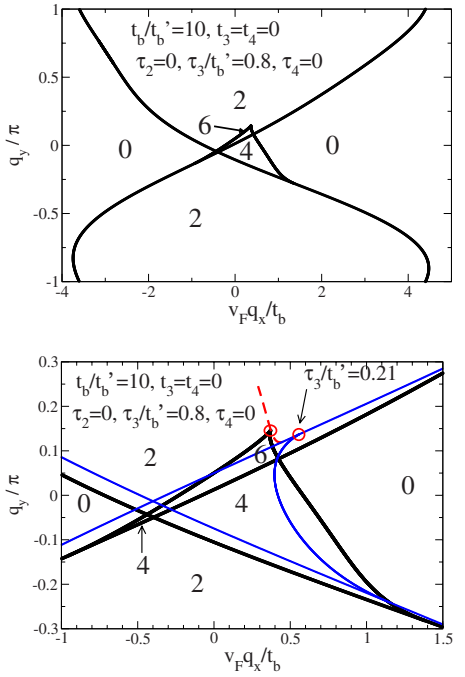

FIG. 4. (Color online) The nesting vector $\mathbf{Q}=\mathbf{q}+\mathbf{Q}_0$ and the number of crossing points. The numbers 0, 2, 4, and 6 mean that there are 0, 2, 4, and 6 crossing points on the Fermi surface with the nesting vector $\mathbf{Q}$. The lower figure is the closeup of the upper figure near $q_x=q_y=0$. Thick lines and thin blue lines in the lower figure are the boundaries for the parameter $\tau_3/t_b'=0.8$ and $\tau_3/t_b'=0.21$, respectively. The red broken line is the trajectory of the edge of the region "6" (red circles) for changing the values of τ_3 (see Fig. 5).

When the Fermi surface and the translated one with vector $\mathbf{Q}$ intersect each other, $\chi_0(\mathbf{Q})$ is large, as we will show in the next section, and the spin density wave (SDW) with vector $\mathbf{Q}$, which gives the largest value of $\chi_0(\mathbf{Q})$, can be stabilized by the electron interaction.

If the order parameter Δ of the spin density wave is finite, the energy becomes

$$E(\mathbf{k}) = \frac{\epsilon_{\mathbf{k}}^{(R)} + \epsilon_{\mathbf{k}-\mathbf{Q}}^{(L)}}{2} \pm \sqrt{\left(\frac{\epsilon_{\mathbf{k}}^{(R)} - \epsilon_{\mathbf{k}-\mathbf{Q}}^{(L)}}{2}\right)^2 + \Delta^2}. \quad (31)$$

When Δ is very small, the energy gap is opened only near the intersection points and there appear the electron pockets and

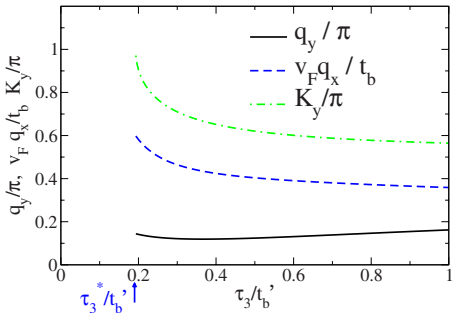

FIG. 5. (Color online) The τ_3 dependence of the edge point of the region "6" (see Fig. 4).

hole pockets depending on the sign of $k_{xF}^{(R)}(k_y)-k_{xF}^{(L)\prime}(k_y)$, as shown in Fig. 3.

When Δ is very small, the areas of electron pockets and hole pockets are given by

$$S_e = \frac{1}{2}\int_{-\pi}^{\pi} (k_{xF}^{(R)}(k_y) - k_{xF}^{(L)\prime}(k_y) + |k_{xF}^{(R)}(k_y) - k_{xF}^{(L)\prime}(k_y)|)dk_y \quad (32)$$

and

$$S_h = \frac{1}{2}\int_{-\pi}^{\pi} [-k_{xF}^{(R)}(k_y) + k_{xF}^{(L)\prime}(k_y) + |k_{xF}^{(R)}(k_y) - k_{xF}^{(L)\prime}(k_y)|]dk_y, \quad (33)$$

respectively. We obtain that the net area of the electron pocket, i.e., the difference of the areas of electron pockets and hole pockets, is obtained as

$$S_e - S_h = -2\pi q_x. \quad (34)$$

When the magnetic field is applied, the x component of the nesting vector (q_x) in FISDW is quantized as

$$q_x = NeB \quad (35)$$

with integer N at low temperature,[29] and the quantized Hall conductivity is labeled by N. The quantization in FISDW may be consistent with the fact that the net area of the electron pocket depends only on q_x, although the explanation of the FISDW is not given completely by the semiclassical picture. This situation is not affected by the presence of ϕ, τ_2, τ_3, and τ_4, as far as we use the linearized dispersion with respect to k_x.

IV. SUSCEPTIBILITY IN QUASI-ONE-DIMENSIONAL SYSTEMS

In this section we study the susceptibility in the quasi-one-dimensional systems. When Hamiltonian is given by

$$\mathcal{H}_0 = \sum_{\mathbf{k},\sigma} \epsilon_{\mathbf{k}} c_{\mathbf{k},\sigma}^{\dagger} c_{\mathbf{k},\sigma}, \quad (36)$$

the static susceptibility is calculated as

$$\chi_0(\mathbf{Q}) = \sum_{\mathbf{k}} \frac{2f[\xi_0(\mathbf{k})]}{\xi_0(\mathbf{k}-\mathbf{Q}) - \xi_0(\mathbf{k})}. \quad (37)$$

Since $\chi_0(-\mathbf{Q})=\chi_0(\mathbf{Q})$, we take $Q_x>0$ without loss of generality. At $T=0$ the integral over k_x can be performed for the quasi-one-dimensional systems with the linearized dispersion [Eqs. (12) and (13)]. Then we obtain

$$\begin{aligned}\chi_0(\mathbf{Q}) &= \int_{-\pi}^{\pi} \frac{dk_y}{2\pi} \int_{k_{xF}^{(L)}(k_y)}^{k_{xF}^{(R)}(k_y)} \frac{dk_x}{2\pi} \frac{2}{\xi_{\mathbf{k}-\mathbf{Q}} - \xi_{\mathbf{k}}} \\ &= \frac{1}{\pi}\int_{-\pi}^{\pi} \frac{dk_y}{2\pi}\left[\int_{k_{xF}^{(L)}(k_y)}^{0} \frac{dk_x}{Y^{(LL)}} + \int_{0}^{k_{xF}^{(R)}(k_y)} \frac{dk_x}{Y^{(LR)} + 2k_x v_F}\right] \\ &= \frac{1}{\pi v_F}\int_{-\pi}^{\pi} \frac{dk_y}{2\pi}\left[\frac{X}{Y^{(LL)}} - \frac{1}{2}\log\left|\frac{Z}{Y^{(LR)}}\right|\right] \end{aligned} \quad (38)$$

where

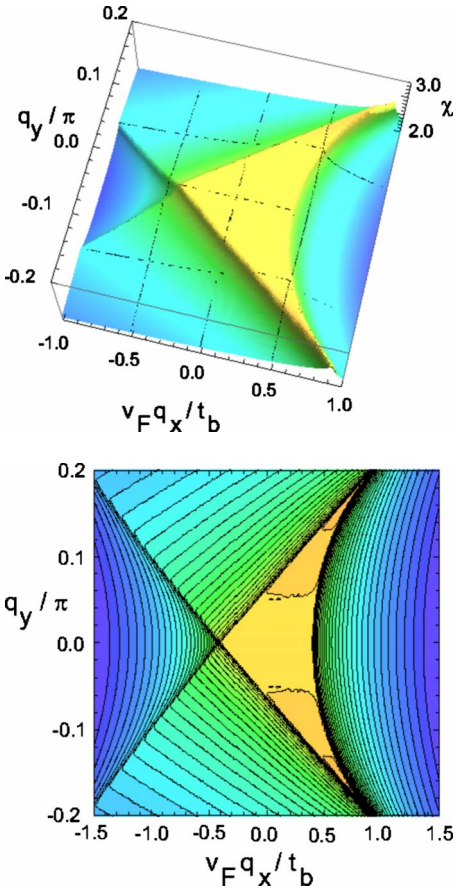

FIG. 6. (Color online) The three-dimensional (3D) plot and the contour plot of $\chi_0(\mathbf{Q})$ as a function of $\mathbf{q}=\mathbf{Q}-\mathbf{Q}_0$ in the quasi-one-dimensional systems with triclinic lattice. The parameters are $t_b'/t_b=0.1$, $t_3=t_4=0$, $\tau_3=\tau_4=0$. The plateaulike maximum of $\chi_0(\mathbf{Q})$ are seen in the region near $q_x=q_y=0$.

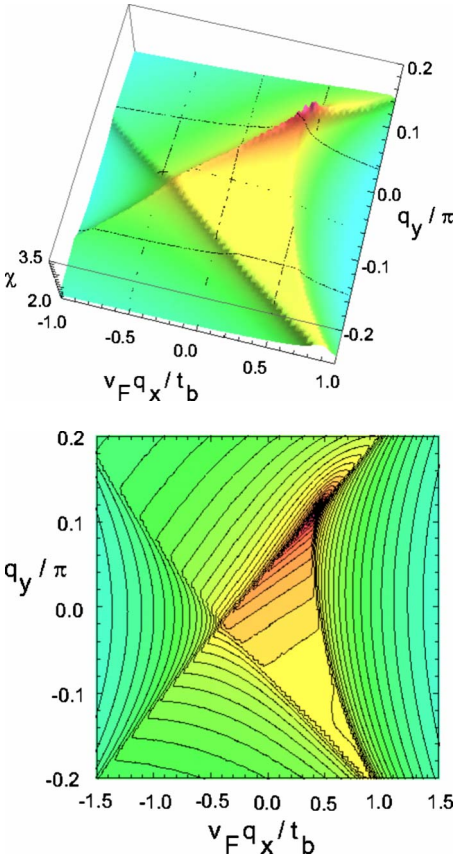

FIG. 7. (Color online) The 3D plot and the contour plot of $\chi_0(\mathbf{Q})$ for the parameters $\tau_3/t_b'=0.3$. Other parameters are the same as taken in Fig. 6. It can be seen that $\chi_0(\mathbf{Q})$ becomes higher at the edge of the plateaulike region in $q_y>0$.

$$X = v_F k_F - t_\perp^{(L)}(k_y), \tag{39}$$

$$Y^{(LL)} = v_F Q_x + t_\perp^{(L)}(k_y - Q_y) - t_\perp^{(L)}(k_y), \tag{40}$$

$$Y^{(LR)} = v_F Q_x + t_\perp^{(L)}(k_y - Q_y) - t_\perp^{(R)}(k_y), \tag{41}$$

and

$$Z = Y^{(LR)} - 2v_F k_x^{(R)}(k_y) = v_F(Q_x - 2k_F) + t_\perp^{(L)}(k_y - Q_y) + t_\perp^{(R)}(k_y). \tag{42}$$

There are kink singularities in the susceptibility at $T=0$ originated from the integral of the logarithm in Eq. (38). The susceptibility has kink when (q_x, q_y) is on the boundary of the regions with the different number of the crossing points. We plot $\chi_0(\mathbf{Q})$ in Figs. 6–9. Note that the susceptibility is symmetric with respect to q_y only when $\tau_2=\tau_3=\tau_4=0$. When $\tau_3 \leq \tau_3^*$, there is no region "6" and $\chi_0(\mathbf{Q})$ has a plateaulike maximum in the region "4," as seen in Fig. 6. With τ_3 larger than the critical value τ_3^*, the two-step plateau in $\chi_0(\mathbf{Q})$ appears in the region "6" as seen in Figs. 7 and 8. The region "6" appears with the t_3 term if t_3 is negative and $|t_3|$ is large as shown in Fig. 9, but the area of higher plateaus is smaller than that in the case with the two-step plateau caused by the τ_3 term.

V. FIELD-INDUCED SPIN DENSITY WAVE

In this section we study the FISDW in the quasi-one-dimensional systems. When the magnetic field is applied in the z direction, we take the Landau gauge,

$$\mathbf{A} = (0, Bx, 0). \tag{43}$$

The wave vector k_x and k_y should be replaced by the operator as

$$\mathbf{k} \to (\mathbf{p} + e\mathbf{A}), \tag{44}$$

where $-e<0$ is the electron charge and

$$\mathbf{p} = -i\nabla. \tag{45}$$

Then the eigenstates in the presence of the magnetic field is obtained by the Schrödinger equation

$$\left[v_F\left(-i\frac{\partial}{\partial x} - k_F\right) + t_\perp^{(R)}\left(-i\frac{\partial}{\partial y} + eBx\right)\right]\Psi^{(R)}(x,y) = E^{(R)}\Psi^{(R)}(x,y), \tag{46}$$

and

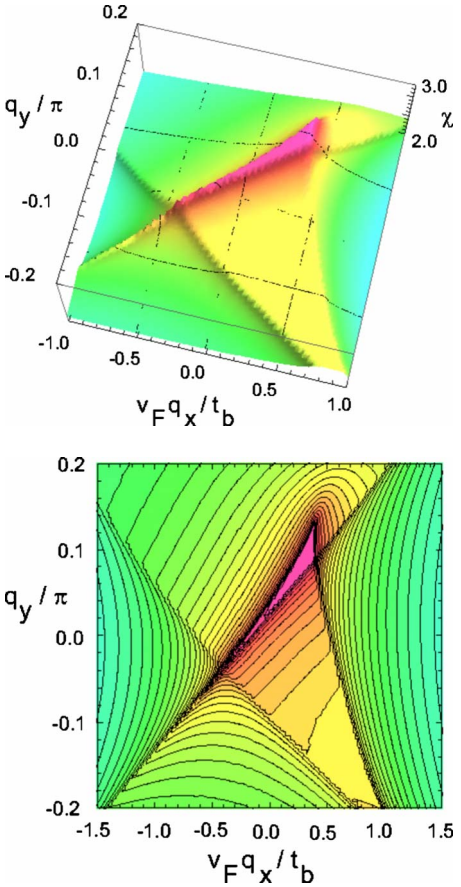

FIG. 8. (Color online) The 3D plot and the contour plot of $\chi_0(\mathbf{Q})$ for the parameters $\tau_3/t_b'=0.6$. Other parameters are the same as taken in Fig. 6. It can be seen that $\chi_0(\mathbf{Q})$ becomes higher at the edge of the plateaulike region in $q_y>0$.

$$\left[v_F\left(i\frac{\partial}{\partial x}-k_F\right)+t_\perp^{(L)}\left(-i\frac{\partial}{\partial y}+eBx\right)\right]\Psi^{(L)}(x,y) = E^{(L)}\Psi^{(L)}(x,y). \tag{47}$$

The eigenstates are obtained as

$$\Psi^{(R)}(x,y) = |(K_x+nG,k_y)^{(R)}\rangle = \exp\left[i\left\{(k_F+K_x+nG)x+k_y y - \frac{1}{v_F G}\int_{k_y}^{k_y+Gx} t_\perp^{(R)}(p)dp\right\}\right], \tag{48}$$

and

$$\Psi^{(L)}(x,y) = |(K_x+nG,k_y)^{(L)}\rangle = \exp\left[i\left\{(-k_F+K_x+nG)x+k_y y + \frac{1}{v_F G}\int_{k_y}^{k_y+Gx} t_\perp^{(L)}(p)dp\right\}\right], \tag{49}$$

where

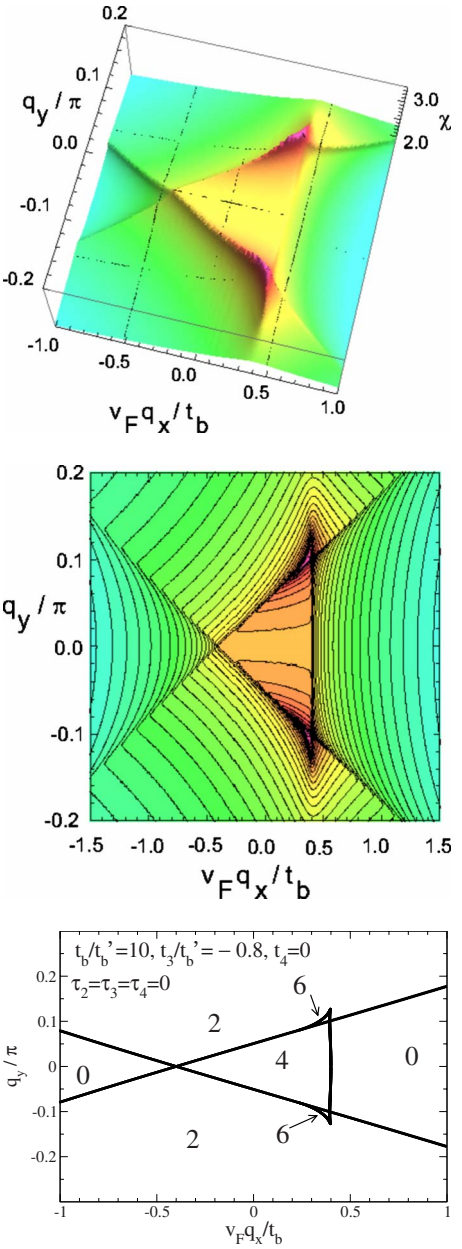

FIG. 9. (Color online) The susceptibility $\chi_0(\mathbf{Q})$ as a function of $\mathbf{q}=\mathbf{Q}-\mathbf{Q}_0$ in the quasi-one-dimensional systems with triclinic lattice. We take $t_3/t_b'=-0.8$ and other parameters are the same as Fig. 6 ($t_b/t_b'=10.0$, $t_4=\tau_3=\tau_4=0$). The region of the six crossing points [Eq. (6)] appears as seen in the figure.

$$G = eB \tag{50}$$

is the width of the Brillouin zone when we take the gauge as Eq. (43). The energy is written as

$$E^{(R)} = v_F(K_x+nG), \tag{51}$$

and

$$E^{(L)} = -v_F(K_x+nG), \tag{52}$$

where n is an integer and

$$0 \le K_x < G. \tag{53}$$

Thus the eigenstate is labeled by K_x, n, and k_y.

The susceptibility is written by using the eigenstates in the magnetic field as

$$\chi_0(\mathbf{Q},B) = \sum_{K_x,n,k_y,K_x',n',k_y'} |\langle (K_x' + n'G + Q_x - 2k_F, k_y' + Q_y)^{(R)} | e^{i\mathbf{Q}\cdot\mathbf{r}} | (K_x + nG, k_y)^{(L)} \rangle|^2 \times \frac{f(E_{K_x+nG}) - f(E_{K_x'+n'G+Q_x-2k_F})}{E_{K_x'+n'G+Q_x-2k_F} - E_{K_x+nG}}. \tag{54}$$

Since we are interested in the case $Q_x \approx 2k_F$, we have taken the matrix element between the left part and the right part and neglected the other matrix elements. With the eigenstates in the magnetic field given in Eqs. (48) and (49), the matrix element is written as

$$|\langle (K_x' + n'G + Q_x - 2k_F, k_y' + Q_y)^{(R)} | e^{i\mathbf{Q}\cdot\mathbf{r}} | (K_x + nG, k_y)^{(L)} \rangle| \equiv \delta_{K_x,K_x'} \delta_{k_y,k_y'} I_{n-n'}(Q_y), \tag{55}$$

where

$$I_{n-n'}(Q_y) = \left| \int_{-\pi}^{\pi} \frac{dp}{2\pi} \exp\left[i \left\{ (n-n')p + \frac{a_1}{G}\sin p + \frac{a_2}{2G}\sin 2p + \frac{a_3}{3G}\sin 3p + \frac{a_4}{4G}\sin 4p \right\} \right] \right| = \left| \sum_{\ell_2=-\infty}^{\infty} \sum_{\ell_3=-\infty}^{\infty} \sum_{\ell_4=-\infty}^{\infty} J_{-n+n'-2\ell_2-3\ell_3-4\ell_4}\left(\frac{a_1}{G}\right) \times J_{\ell_2}\left(\frac{a_2}{2G}\right) J_{\ell_3}\left(\frac{a_3}{3G}\right) J_{\ell_4}\left(\frac{a_4}{4G}\right) \right|. \tag{56}$$

We obtain

$$\chi_0(\mathbf{Q},B) = \sum_N |I_N(Q_y)|^2 \chi_0^{1D}(Q_x - NG), \tag{57}$$

where $\chi_0^{1D}(Q_x+NG)$ is the susceptibility in the one-dimensional system given by

$$\chi_0^{1D}(Q_x - NG) = N(0) \int_{-\xi_c}^{\xi_c} d\xi \times \frac{f\left(-\xi + \frac{1}{2}\epsilon^{1D}_{Q_x-NG-2k_F}\right) - f\left(\xi + \frac{1}{2}\epsilon^{1D}_{Q_x-NG-2k_F}\right)}{2\xi}, \tag{58}$$

where

$$\epsilon^{1D}_{Q_x-NG-2k_F} = v_F(Q_x - NG - 2k_F). \tag{59}$$

When the magnetic field is finite, the susceptibility in the quasi-one-dimensional system is given in terms of the one-dimensional susceptibility, which diverges logarithmically for $Q_x=NG+2k_F$ at $T=0$. The quantization of Q_x is caused by this divergence of the susceptibility at $T=0$. At finite but small T, the maximum of $\chi_0(\mathbf{Q})$ is obtained at $\mathbf{Q}$ which gives the maximum of $I_N(Q_y)$ and $Q_x=2k_F+NG$.

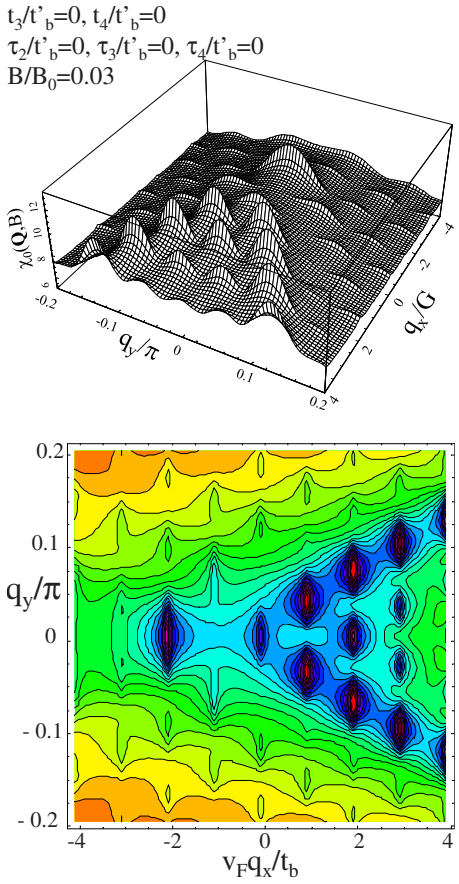

FIG. 10. (Color online) The 3D plot and the contour plot of the wave-vector-dependent susceptibility in the magnetic field.

We take the unit of the magnetic field as

$$B_0 = \frac{4t_b}{v_F e}, \tag{60}$$

i.e., $B_0 \approx 400$ T for $(TMTSF)_2PF_6$ and $(TMTSF)_2ClO_4$. We plot the susceptibility at $B=0.03B_0$ and $T=0.001t_b$ as a function q_x and q_y in Figs. 10 and 11. The susceptibilities as a function of the magnetic field B are plotted in Fig. 12, where the wave vector $\mathbf{Q}$ is taken to give the maximum value of $\chi_0(\mathbf{Q})$ for given B, i.e., Q_x is quantized to be $q_x=Q_x-2k_F=NeB$ with integer N and Q_y is searched numerically to give the absolute maximum of $\chi_0(\mathbf{Q})$ for each N. As seen in Fig. 12, $\chi_0(\mathbf{Q},B)$ for $N\neq 0$ is enhanced by τ_3 but that for $N=0$ is not. This effect of τ_3 on $\chi_0(\mathbf{Q},B)$ can be interpreted as follows. As mentioned above, the wave vector $\mathbf{q}$ for $N\neq 0$ locates in the region "6" or near that region. The susceptibility at $B=0$ is enhanced in the region "6" as we have discussed in the previous section. Therefore, it is natural to expect that $\chi_0(\mathbf{Q},B)$ with $N\neq 0$ is also enhanced. On the other hand, the wave vector $\mathbf{q}$ for the peak of the $\chi_0(\mathbf{Q},B)$ with $N=0$ is given at $q_x=0$ and q_y goes to $q_y=0$ as B becomes large. Since $\mathbf{q}=(0,0)$ is in the region "4," where $\chi_0(\mathbf{Q})$ at $B=0$ is little affected by τ_3 term. This may explain the small effect of τ_3 on $\chi_0(\mathbf{Q},B)$ with $N=0$.

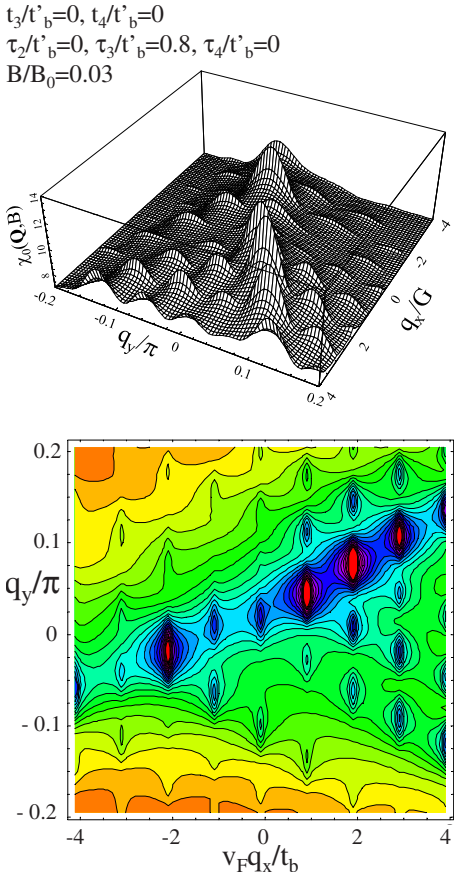

FIG. 11. (Color online) The same as Fig. 10 with finite τ_3. The susceptibility is not symmetric with respect q_y.

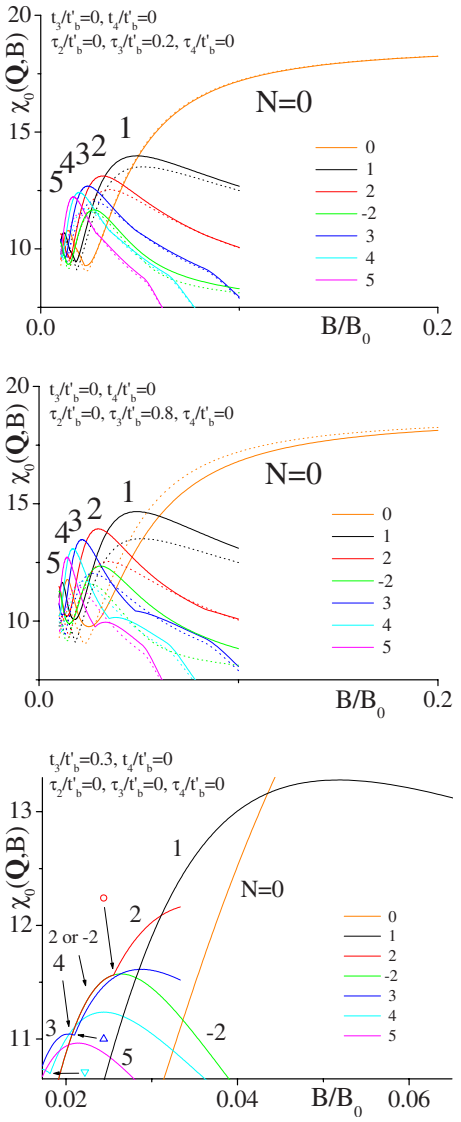

FIG. 12. (Color online) The susceptibility $\chi_0(\mathbf{Q},B)$ as a function of B. We take $Q_x=2k_F+NG$ with integer N and vary $q_y=Q_y-\pi-\phi$ to get the maximum value of $\chi_0(\mathbf{Q},B)$ for given N and B. The dotted lines are obtained by taking $\tau_3=0$, and the solid lines are obtained by taking $\tau_3/t_b'=0.2$ (upper figure), $\tau_3/t_b'=0.8$ (middle figure), and $t_3/t_b'=0.3$ (lower figure). Other parameters are set to be zero except for $t_b'/t_b=0.1$.

In Fig. 13 we plot the nesting vector $\mathbf{q}=\mathbf{Q}-\mathbf{Q}_0$ for various values of B. In these figures the wave vectors for each quantized q_x are plotted, which do not always give the absolute maximum of $\chi_0(\mathbf{Q})$. For $\tau_3/t_b'=0.2$ (the upper figure in Fig. 13), the region "6" is very small and invisible in this scale. Even in that case, the nesting vectors for $N>0$ locate near the upper edge of the region "4," where the new plateau will appear for the larger values of τ_3. When τ_3 is large enough to make the two-step plateau, the wave vectors are located in the region "6" for most of the cases as seen in the middle figures in Fig. 13. As the magnetic field becomes larger, q_x for $N\neq 0$ becomes larger and $\mathbf{q}$ cannot be in the region "6." Then $\mathbf{q}$ locates in the region "2" with $q_y>0$ but further increase of B makes the jump of $\mathbf{q}$ into region of "4" with $q_y<0$. We plot the phase diagram for the index N of FISDW in the plane of the magnetic field and τ_3/t_b' (the upper figure), τ_2/t_b' (the middle figure), or t_3/t_b' (the lower figure) in Fig. 14. The region of FISDW state with $N=0$ is shifted toward the higher magnetic field, as $|\tau_3|$ increases, which can be understood by noting that the FISDW states with $N\neq 0$ are enhanced by τ_3 term but that with $N=0$ is not. The boundary of the FISDW states with different N is less affected by τ_2 than by τ_3. The effects of t_3 term on the susceptibility and the phase boundary of FISDW with different N are also smaller than those of τ_3 term, as shown in the lower figure in Fig. 14. The reason can be seen in Eqs. (27) and (28) since $q_y\approx 0$, τ_3 term is more important than τ_2 and t_3 terms, which are proportional to $\sin q_y$ and $\sin(3q_y/2)$, respectively, and are small for small q_y. The phase boundary near $t_3/t_b'\approx 0.3$ are caused by the jump of the nesting vector $\mathbf{q}$ when the magnetic field is changed, as seen in the lower figure in Fig. 13. The local maximum of $\chi_0(\mathbf{Q},B)$ locates at $q_y=0$ for the even number N, when $\tau_2=\tau_3=0$. When t_3 is larger than the critical value, the local maximum at $q_y=0$ may become the largest. In that case the peaks at $\pm N$ have the same value, as we write "2 or −2" in the lower figure in Fig. 14. This degeneracy can be lifted by t_4 term[28] or τ_3 term, but the degeneracy of $N=2$ and $N=-2$ at $q_y=0$ is not lifted by τ_2 term.

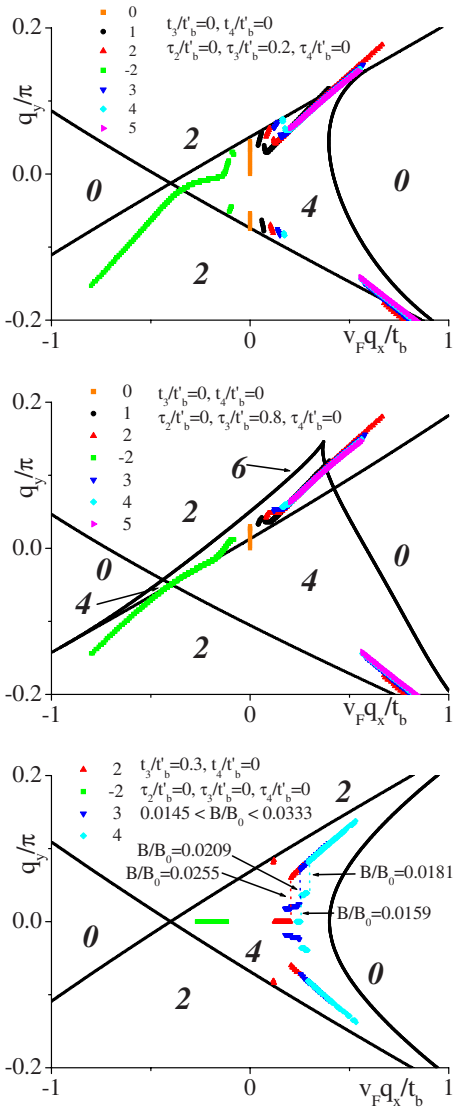

FIG. 13. (Color online) The nesting vector of the FISDW in quasi-one-dimensional systems with parameter τ_3/t'_b=0.2 (the upper figure), τ_3/t'_b=0.8 (the middle figure) and t_3/t'_b=0.3 (the lower figure). We take t'_b/t_b=0.1 and other parameters are set to be zero.

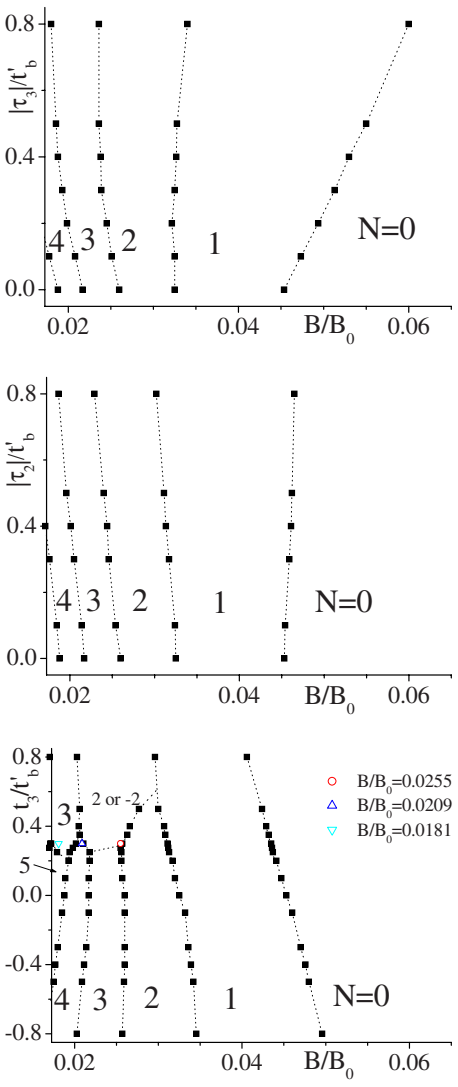

FIG. 14. (Color online) Phase diagram for the index N of the FISDW in the plane of the magnetic field and the parameter τ_3/t'_b (the upper figure) or τ_2/t'_b (the middle figure), and t_3 (the lower figure). Other parameters are set to be zero except for t'_b/t_b=0.1.

VI. CONCLUSION

We have studied the susceptibility in the quasi-one-dimensional systems theoretically. We find the two-step plateaulike maximum of $\chi_0(\mathbf{Q})$ at B=0 in the case of the warped Fermi surface with $\mp 2\tau_3 \sin 3(k_y \mp \phi)$ term, which is expected to exist in the triclinic lattice. The susceptibility is much enhanced in the higher plateaulike region (the region "6"), where the Fermi surface intersects with the translated one at six points, while the intersection points are four in the lower plateau region (the region "4"). The susceptibility in the presence of the magnetic field $\chi_0(\mathbf{Q},B)$ is also studied. The FISDW states are labeled by the integer N, which corresponds to the peaks of $\chi_0(\mathbf{Q},B)$ at the quantized value of $q_x=NG$. Even in that case $\chi_0(\mathbf{Q},B)$ is shown to be large when $\mathbf{q}$ locates in the plateaulike maximum region at B=0. This feature explains the relatively strong dependence of the phase boundary between N=0 and N=1 on τ_3 (the N=1 phase is realized in the larger range of the magnetic field as $|\tau_3|$ increases.) than on τ_2 and t_3. Since the parameters t_b, t'_b, t_3, τ_2, and τ_3 are expected to be strongly affected by pressure, the experimental study[30,31] of the pressure dependence of the phase boundaries in the FISDW states will reveal the importance of the τ_3 in the quasi-one-dimensional systems, although it is difficult to predict on what conditions the enhancement of the wave-vector-dependent susceptibility will be observed experimentally.

In this paper we have not taken account of the periodic potential caused by the anion ordering. The interplay between the periodic potential and the warping of the Fermi surface studied in this paper is interesting.

The nesting properties studied in this paper are also important for the presence of the superconductivity with the finite total momentum of Cooper pairs, [Fulde-Ferrel-Larkin-Ovchinnikov (FFLO) state],[32] which is proposed to exist in $(TMTSF)_2ClO_4$.[33]

APPENDIX: TIGHT-BINDING MODEL FOR FIG. 1

In this Appendix we show how Eqs. (12)–(14) are derived from the tight-binding model on the triclinic lattice in Fig. 1. Note that there are two nonequivalent sites in the unit cell (right triangles and left triangles in Fig. 1), and the unit lattice vectors are $2\mathbf{a}$ and $\mathbf{b}$. The Hamiltonian for the tight-binding model is given as

$$\mathcal{H} = \sum_{\mathbf{k}} (c_{1,\mathbf{k}}^{\dagger}, c_{2,\mathbf{k}}^{\dagger}) \begin{pmatrix} \mathcal{H}_{11} & \mathcal{H}_{12} \\ \mathcal{H}_{21} & \mathcal{H}_{22} \end{pmatrix} \begin{pmatrix} c_{1,\mathbf{k}} \\ c_{2,\mathbf{k}} \end{pmatrix}, \tag{A1}$$

where

$$\mathcal{H}_{11} = \mathcal{H}_{22} = 2I_3 \cos k_y + 2I_4 \cos(k_y - 2k_x) - \epsilon_F, \tag{A2}$$

$$\mathcal{H}_{12} = \mathcal{H}_{21}^{*} = S_1 e^{ik_x} + S_2 e^{-ik_x} + I_1 e^{i(k_x - k_y)} + I_2 e^{-i(k_x - k_y)}, \tag{A3}$$

$$k_x = \mathbf{k} \cdot \mathbf{a}, \tag{A4}$$

and

$$k_y = \mathbf{k} \cdot \mathbf{b}. \tag{A5}$$

The energy is obtained as

$$\epsilon_{\mathbf{k}} = \mathcal{H}_{11} \pm |\mathcal{H}_{12}|. \tag{A6}$$

Since we consider the 3/4 filled band, we take the upper band. Then we obtain,

$$\begin{aligned} \epsilon_{\mathbf{k}} &= 2I_3 \cos k_y + 2I_4 \cos(k_y - 2k_x) \\ &\quad + \{[2S \cos k_x + 2T \cos(k_x - k_y)]^2 \\ &\quad + [2\Delta S \sin k_x + 2\Delta T \sin(k_x - k_y)]^2\}^{1/2} - \epsilon_F, \end{aligned} \tag{A7}$$

where

$$S = \frac{1}{2}|S_1 + S_2|, \tag{A8}$$

$$\Delta S = \frac{1}{2}(S_1 - S_2), \tag{A9}$$

$$T = \frac{1}{2}\mathrm{sgn}(S)(I_1 + I_2), \tag{A10}$$

$$\Delta T = \frac{1}{2}(I_1 - I_2). \tag{A11}$$

For the quasi-one-dimensional systems, we can take S much larger than $|\Delta S|$, $|T|$, $|\Delta T|$, $|I_3|$ and $|I_4|$. For the zeroth order and the first order in ΔS, T, ΔT, I_3, and I_4, we obtain

$$\begin{aligned} \epsilon_{\mathbf{k}}^{(1)} &= |2S \cos k_x + 2T \cos(\pm k_F' - k_y)| + 2I_3 \cos k_y \\ &\quad + 2I_4 \cos(k_y \mp 2k_F') - \epsilon_F \\ &\approx 2S(\cos k_x - \cos k_F') - 2t_1 \cos k_y \pm 2\tau_1 \sin k_y \\ &= -v_F(|k_x| - k_F') - 2t_b \cos(k_y \pm \phi), \end{aligned} \tag{A12}$$

where $k_F' = \pi/4$ is the Fermi wave number in the first Brillouin zone,

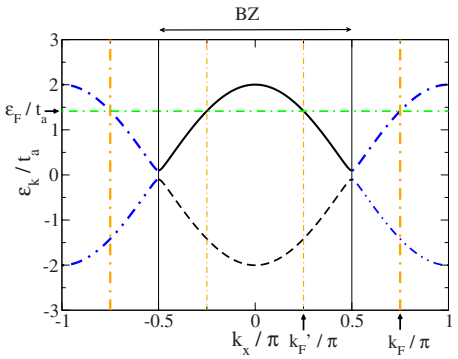

FIG. 15. (Color online) Schematic figure of the quasi-one-dimensional band as a function of k_x for the fixed value of k_y.

$$v_F = \sqrt{2}S, \tag{A13}$$

$$t_1 = -I_3 - \frac{\sqrt{2}}{2}T, \tag{A14}$$

$$\tau_1 = I_4 + \frac{\sqrt{2}}{2}T, \tag{A15}$$

$$t_b = \mathrm{sgn}(t_1)\sqrt{t_1^2 + \tau_1^2}, \tag{A16}$$

and

$$\phi = \arctan\frac{\tau_1}{t_1}. \tag{A17}$$

In the above the principal value of arctangent should be taken ($|\phi| \le \pi/2$).

In the extended zone we take the Fermi wave number as $k_F = 3\pi/4$ (see Fig. 15). Then we obtain

$$\epsilon_{\mathbf{k}}^{(1)} = v_F(|k_x| - k_F) - 2t_b \cos(k_y \mp \phi), \tag{A18}$$

for $|k_x| \approx k_F$. Note that the sign of t_b and ϕ is different from those studied by Yamaji,[1,24] where the first Brillouin zone is used.

Next, we consider the higher order terms in I_3/S, I_4/S, $\Delta S/S$, T/S, and $\Delta S/S$. We expand in Eq. (A7) as

$$\begin{aligned} \epsilon_{\mathbf{k}} &\approx \epsilon_{\mathbf{k}}|_{k_x = \pm k_F'} + \left.\frac{\partial \epsilon_{\mathbf{k}}}{\partial k_x}\right|_{k_x = \pm k_F'} (k_x \mp k_F') \\ &\quad + \frac{1}{2!}\left.\frac{\partial^2 \epsilon_{\mathbf{k}}}{\partial k_x^2}\right|_{k_x = \pm k_F'} (k_x \mp k_F')^2 + \frac{1}{3!}\left.\frac{\partial^3 \epsilon_{\mathbf{k}}}{\partial k_x^3}\right|_{k_x = \pm k_F'} (k_x \mp k_F')^3 \\ &\quad + \cdots \end{aligned} \tag{A19}$$

To obtain the second order terms in ΔS, T, ΔT, and I_4, we expand $\epsilon_{\mathbf{k}}|_{k_x = \pm k_F}$ and $\frac{\partial \epsilon_{\mathbf{k}}}{\partial k_x}|_{k_x = \pm k_F}$ in these parameters and we set

$$|k_x| - k_F' = -\frac{2t_b}{v_F}\cos(k_y \pm \phi) + O\left[\left(\frac{I_3}{S}\right)^2, \cdots\right], \tag{A20}$$

in Eq. (A19). Then we obtain[1,24]

$$\epsilon_{\mathbf{k}}^{(2)} = -v_F(|k_x| - k_F') - 2t_b \cos(k_y \pm \phi) - 2t_b' \cos 2(k_y \pm \phi) \pm 2\tau_2 \sin 2(k_y \pm \phi), \tag{A21}$$

where

$$t_b' = \frac{\sqrt{2}}{4S}[4I_3I_4 + \sqrt{2}T(I_3 + I_4) - (\Delta T)^2 \sin 2\phi + t_b^2], \tag{A22}$$

and

$$\tau_2 = \frac{\sqrt{2}}{4S}[2T^2 + 4I_4^2 + \sqrt{2}T(I_3 + 3I_4) - (\Delta T)^2 \cos 2\phi]. \tag{A23}$$

We have neglected the k_y-independent terms, because these terms are the corrections of ϵ_F and they are not important in our study. Taking

$$|k_x| - k_F' \approx \frac{1}{v_F}\{-2t_b \cos(k_y \pm \phi) - 2t_b' \cos[2(k_y \pm \phi)] \pm 2\tau_2 \sin[2(k_y \pm \phi)]\}, \tag{A24}$$

we obtain t_3 and τ_3 in the third order expansion as

$$t_3 = -\frac{\sqrt{2}I_4(t_b' \cos\phi + \tau_2 \sin\phi)}{S} - \frac{2I_4 t_b^2 \sin\phi}{S^2} + \frac{(\Delta T)^2 t_b(2\cos 2\phi + \sin 2\phi)}{4S^2} + \frac{\sqrt{2}T(\Delta T)^2(\cos 3\phi + \sin 3\phi)}{8S^2} + \frac{\sqrt{2}t_b t_b'}{2S} - \frac{T[t_b'(\cos\phi + \sin\phi) - \tau_2(\cos\phi - \sin\phi)]}{2S} + \frac{\sqrt{2}Tt_b^2(\cos\phi - \sin\phi)}{8S^2} + \frac{t_b^3}{12S^2}, \tag{A25}$$

and

$$\tau_3 = \frac{\sqrt{2}I_4(t_b' \sin\phi - \tau_2 \cos\phi)}{S} - \frac{2I_4 t_b^2 \cos\phi}{S^2} + \frac{(\Delta T)^2 t_b(\cos 2\phi - 2\sin 2\phi)}{4S^2} + \frac{\sqrt{2}T(\Delta T)^2(\cos 3\phi - \sin 3\phi)}{8S^2} + \frac{\sqrt{2}t_b\tau_2}{2S} - \frac{T[t_b'(\cos\phi - \sin\phi) + \tau_2(\cos\phi + \sin\phi)]}{2S} - \frac{\sqrt{2}Tt_b^2(\cos\phi + \sin\phi)}{8S^2}. \tag{A26}$$

Although there exist the third order corrections in t_b and ϕ, we can neglect these corrections. When we use the transfer integrals for $(TMTSF)_2ClO_4$ obtained by the *ab initio* calculation by Ishibashi *et al.*[23] (S_1=263.0 meV, S_2=237.0 meV, I_1=−19.1 meV, I_2=−41.8 meV, I_3=53.2 meV, and I_4=−4.70 meV), we obtain t_b=−41.1 meV, ϕ=39.6°, t_b'=−2.16 meV, τ_2=0.332 meV, t_3=0.0419 meV, and τ_3=0.470 meV (t_b'/t_b=0.0526, τ_2/t_b'=−0.154, t_3/t_b'=−0.0194, and τ_3/t_b'=−0.218). In this case the value of $|\tau_3/t_b'|$ is near the critical value discussed in the text. When we use the parameters obtained by Ducasse *et al.*[22] for $(TMTSF)_2ClO_4$ at 7 K (S_1=287 meV, S_2=266 meV, I_1=−34.0 meV, I_2=−64.1 meV, I_3=46.2 meV, and I_4=7.5 meV), we obtain t_b=−29.5 meV, ϕ=67.0°, t_b'=−2.09 meV, τ_2=0.548 meV, t_3=−0.132 meV, and τ_3=0.163 meV (t_b'/t_b=0.07, τ_2/t_b'=−0.262, t_3/t_b'=−0.063, and τ_3/t_b'=−0.078). When the parameters for $(TMTSF)_2PF_6$ at 4 K (Ref. 22) (S_1=280 meV, S_2=254 meV, I_1=−17.8 meV, I_2=−49.7 meV, I_3=46.9 meV, and I_4=5.6 meV) are used, we obtain t_b=−29.5 meV, ϕ=36.7°, t_b'=−0.972 meV, τ_2=−0.981 meV, t_3=−0.128 meV, and τ_3=0.038 meV (t_b'/t_b=0.03, τ_2/t_b'=1.01, t_3/t_b'=0.132, and τ_3/t_b'=0.039). In these cases $|\tau_3/t_b'|$ is smaller than the critical value $|\tau_3^*/t_b'|$.

In the similar way we can obtain t_4 and τ_4, and we get Eqs. (12)–(14), but we take t_3, τ_3, t_4 and τ_4 as independent parameters in this paper.

[1] T. Ishiguro, K. Yamaji, and G. Saito, *Organic Superconductors*, 2nd ed. (Springer-Verlag, Berlin, 1998). We use the different sign notation from the right hand side of Eq. (4.53) in that book.

[2] *The Physics of Organic Superconductors and Conductors*, edited by A. G. Lebed (Springer, New York, 2008).

[3] L. P. Gor'kov and A. G. Lebed, J. Phys. (Paris), Lett. **45**, 433 (1984).

[4] G. Montambaux, M. Heritier, and P. Lederer, Phys. Rev. Lett. **55**, 2078 (1985).

[5] K. Yamaji, J. Phys. Soc. Jpn. **54**, 1034 (1985).

[6] A. G. Lebed', Sov. Phys. JETP **62**, 595 (1985).

[7] K. Maki, Phys. Rev. B **33**, 4826 (1986).

[8] A. Virosztek, L. Chen, and K. Maki, Phys. Rev. B **34**, 3371 (1986).

[9] L. Chen and K. Maki, Phys. Rev. B **35**, 8462 (1987).

[10] K. Yamaji, J. Phys. Soc. Jpn. **56**, 1841 (1987).

[11] N. Biskup, J. S. Brooks, R. Kato, and K. Oshima, Phys. Rev. B **60**, R15005 (1999).

[12] K. Oshima, T. Sasaki, M. Motokawa, and R. Kato, Synth. Met. **120**, 943 (2001).

[13] A. G. Lebed and P. Bak, Phys. Rev. B **40**, 11433 (1989).

[14] T. Osada, S. Kagoshima, and N. Miura, Phys. Rev. Lett. **69**, 1117 (1992).

[15] Y. Hasegawa, K. Kishigi, and M. Miyazaki, J. Phys. Soc. Jpn.

67, 964 (1998).
[16] M. Miyazaki, K. Kishigi, and Y. Hasegawa, J. Phys. Soc. Jpn. **68**, 313 (1999).
[17] D. Radić, A. Bjelis, and D. Zanchi, Phys. Rev. B **69**, 014411 (2004).
[18] S. Haddad, S. Charfi-Kaddour, M. Heritier, and R. Bennaceur, Phys. Rev. B **72**, 085104 (2005).
[19] D. Zanchi and A. Bjelis, EPL **56**, 596 (2001).
[20] K. Sengupta and N. Dupuis, Phys. Rev. B **65**, 035108 (2001).
[21] K. Kishigi and Y. Hasegawa, Phys. Rev. B **80**, 075119 (2009).
[22] L. Ducasse, M. Abderrabba, J. Hoarau, M. Pesquer, B. Gallois, and J. Gaultier, J. Phys. C **19**, 3805 (1986).
[23] S. Ishibashi, A. A. Manuel, and M. Kohyama, J. Phys.: Condens. Matter **11**, 2279 (1999).
[24] K. Yamaji, J. Phys. Soc. Jpn. **55**, 860 (1986).
[25] Y. Hasegawa and K. Kishigi, Phys. Rev. B **78**, 045117 (2008).
[26] M. Héritier, G. Montambaux, and P. Lederer, J. Phys. (Paris), Lett. **45**, 943 (1984).
[27] A. G. Lebed, Pis'ma Zh. Eksp. Teor. Fiz. **78**, 170 (2003) [JETP Lett. **78**, 138 (2003)].
[28] D. Zanchi and G. Montambaux, Phys. Rev. Lett. **77**, 366 (1996).
[29] A. G. Lebed, Phys. Rev. Lett. **88**, 177001 (2002).
[30] A. V. Kornilov, V. M. Pudalov, Y. Kitaoka, K. Ishida, T. Mito, J. S. Brooks, J. S. Qualls, J. A. A. J. Perenboom, N. Tateiwa, and T. C. Kobayashi, Phys. Rev. B **65**, 060404(R) (2002).
[31] W. Kang, S. T. Hannahs, and P. M. Chaikin, Phys. Rev. Lett. **70**, 3091 (1993).
[32] M. Miyazaki, K. Kishigi, and Y. Hasegawa, J. Phys. Soc. Jpn. **68**, 3794 (1999).
[33] S. Yonezawa, S. Kusaba, Y. Maeno, P. Auban-Senzier, C. Pasquier, K. Bechgaard, and D. Jerome, Phys. Rev. Lett. **100**, 117002 (2008).